Figures and figure supplements

Lactate is an energy substrate for rodent cortical neurons and enhances their firing activity

Anastassios Karagiannis *et al*

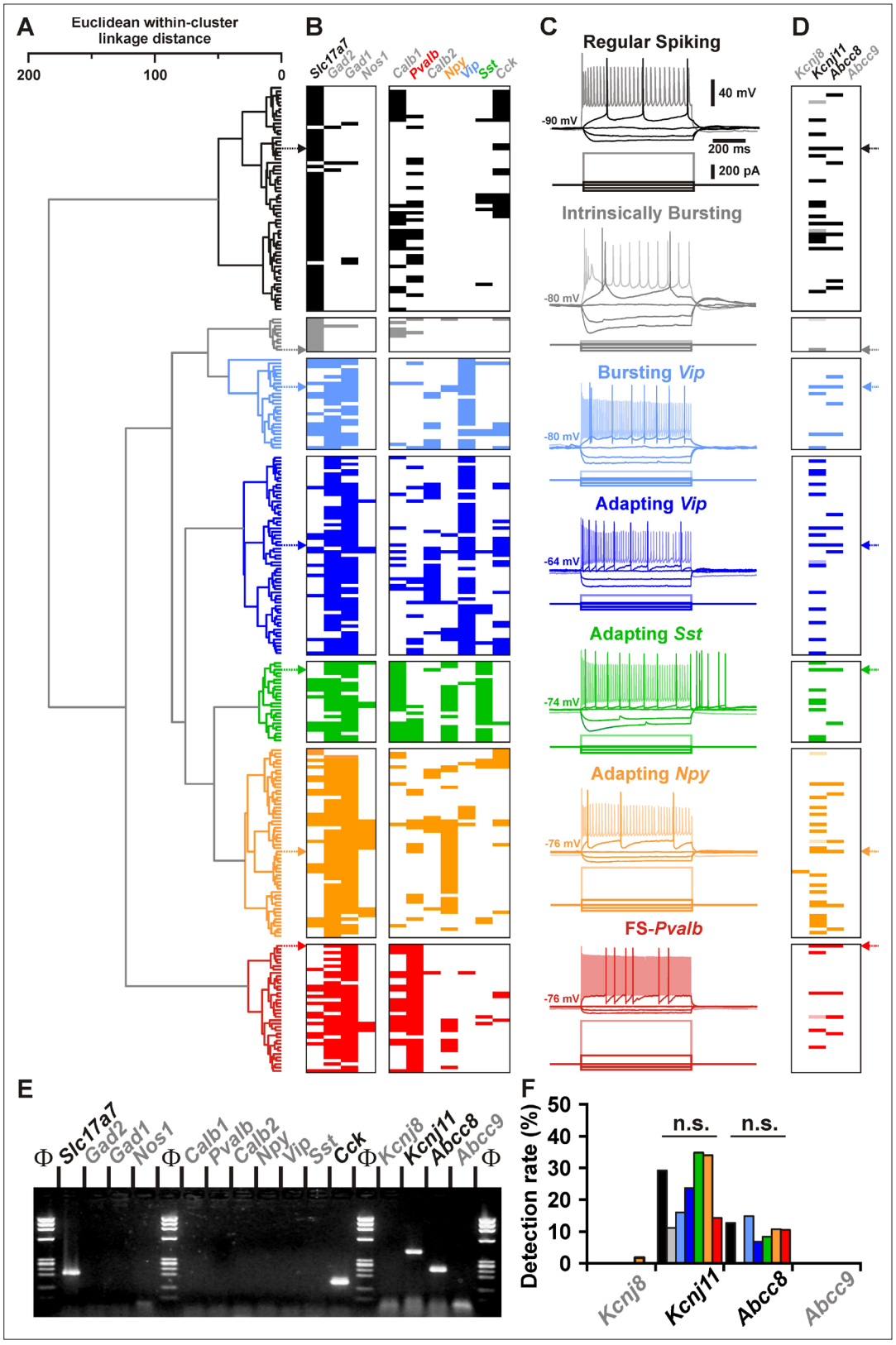

Figure 1. Detection of *Kcnj11* and *Abcc8* K_{ATP} channel subunits in cortical neuron subtypes. (**A**) Ward's clustering of 277 cortical neurons (left panel). The *x*-axis represents the average within-cluster linkage distance, and the *y*-axis the individuals. (**B**) Gene detection profile across the different cell clusters. For each cell, colored and white rectangles indicate presence and absence of genes, respectively. (**C**) Representative voltage responses induced by

Figure 1 continued on next page

Figure 1 continued

injection of current pulses (bottom traces) corresponding to −100, −50, and 0 pA, rheobase and intensity inducing a saturating firing frequency (shaded traces) of a regular spiking neuron (black), an intrinsically bursting neuron (gray), a bursting vasoactive intestinal polypeptide (*Vip*) interneuron (light blue), an adapting *Vip* interneuron (blue), an adapting *Sst* interneuron (green), an adapting *Npy* interneuron (orange), and a **Fast Spiking-Parvalbumin interneuron** (FS-*Pvalb*, red). The colored arrows indicate the expression profiles of neurons whose firing pattern is illustrated in (**C**). (**D**) Detection of the subunits of the K_{ATP} channels in the different clusters. Shaded rectangles represent potential *Kcnj11* false positives in which genomic DNA was detected in the harvested material. (**E**) Single-cell RT-PCR (scRT-PCR) analysis of the regular spiking (RS) neuron depicted in (**A–D**). (**F**) Histograms summarizing the detection rate of K_{ATP} channel subunits in identified neuronal types. n.s., not statistically significant.

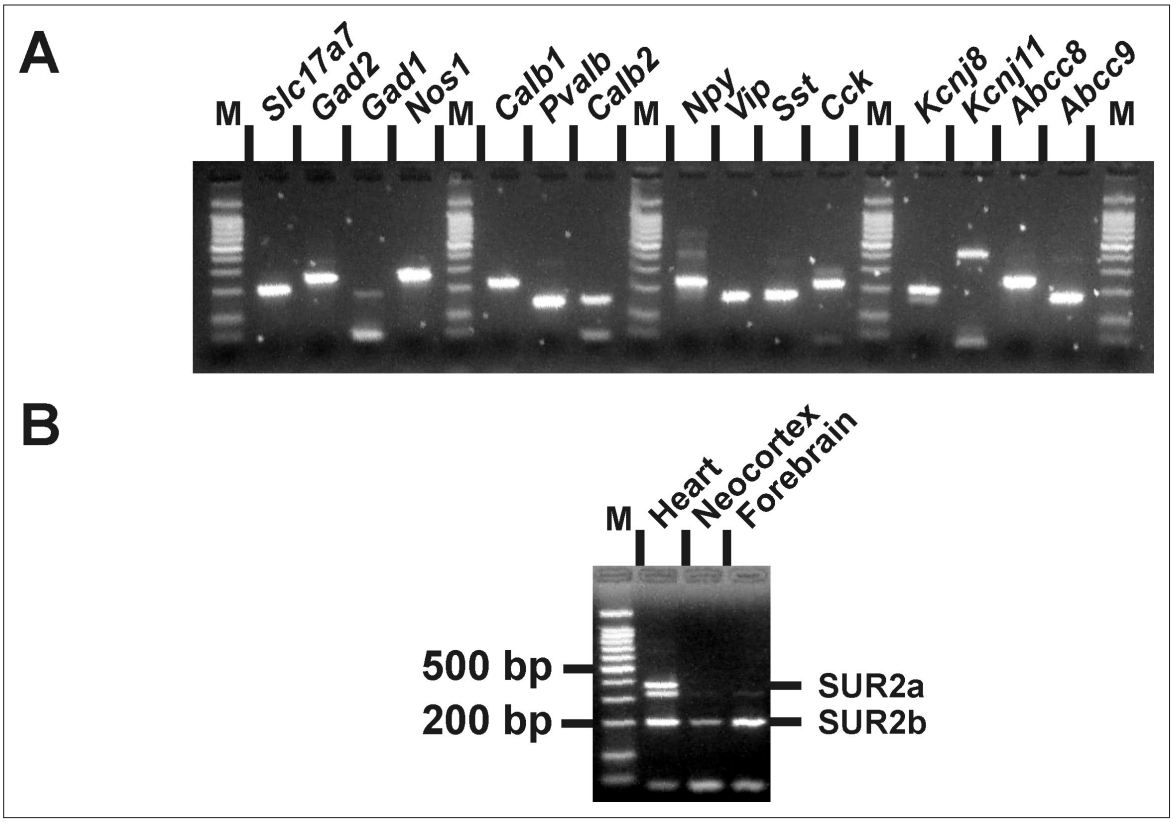

Figure 1—figure supplement 1. Molecular expression of K_{ATP} channels. (**A**) RT-PCR products generated from 500 pg of total cortical RNAs. M: 100 bp ladder molecular weight marker. (**B**) *Abcc9* splice variants-specific RT-PCR analysis of 1 ng total RNAs from rat heart, neocortex, and forebrain.

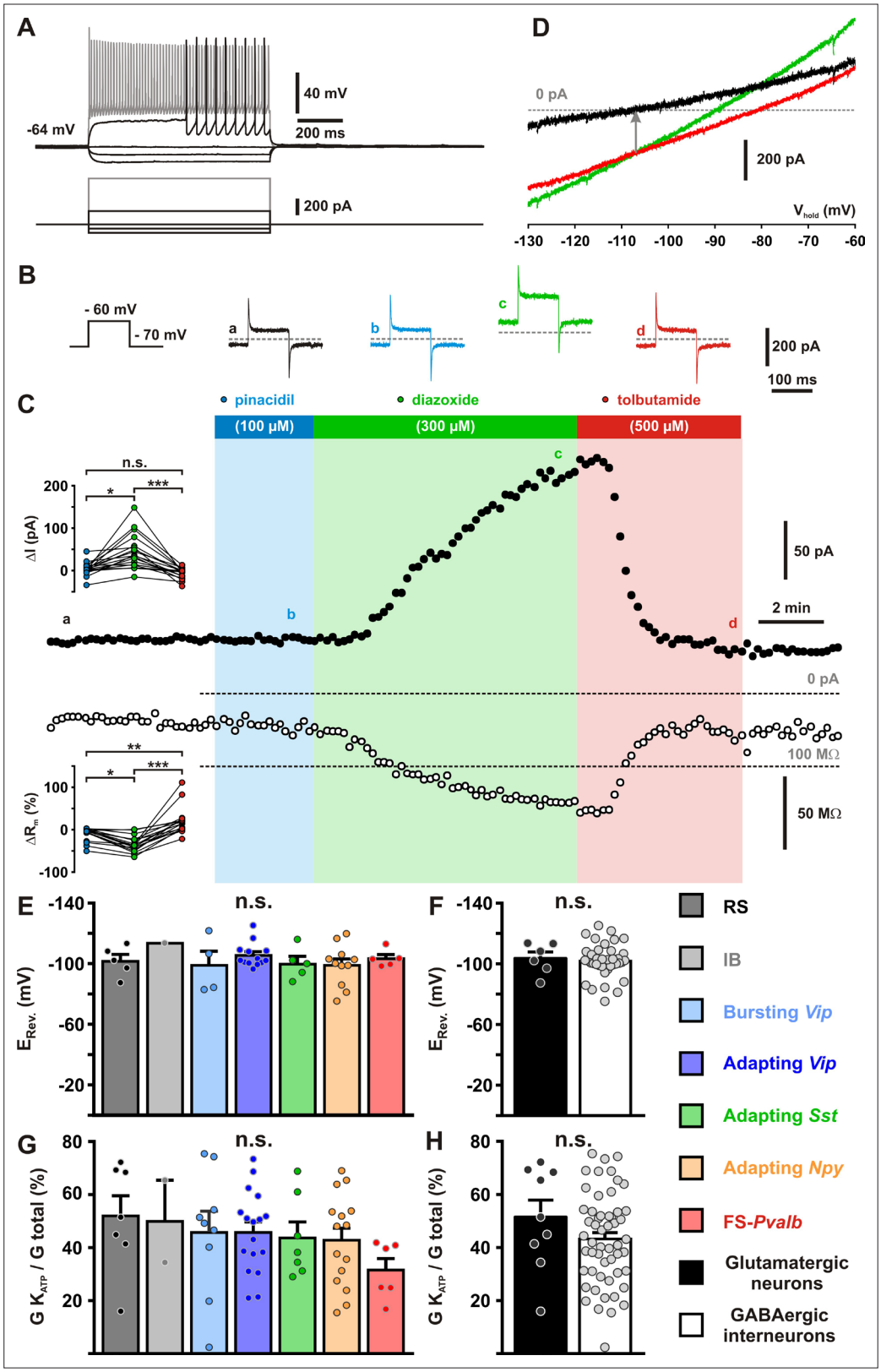

Figure 2. Pharmacological and biophysical characterization of K_{ATP} channels in cortical neurons. (**A**) Representative voltage responses of a Fast Spiking-Parvalbumin (FS-*Pvalb*) interneuron induced by injection of current pulses (bottom traces). (**B**) Protocol of voltage pulses from −70 to −60 mV (left trace). Responses of whole-cell currents in the FS-*Pvalb* interneurons shown in (**A**) in control condition (black) and in presence of pinacidil (blue), piazoxide

Figure 2 continued on next page

Figure 2 continued

(green) and tolbutamide (red) at the time indicated by a–d in (**C**). (**C**) Stationary currents recorded at −60 mV (filled circles) and membrane resistance (open circles) changes induced by K_{ATP} channel modulators. The colored bars and shaded zones indicate the duration of application of K_{ATP} channel modulators. Upper and lower insets: changes in whole-cell currents and relative changes in membrane resistance induced by K_{ATP} channel modulators, respectively. (**D**) Whole-cell current–voltage relationships measured under diazoxide (green trace) and tolbutamide (red trace). K_{ATP} *I/V* curve (black trace) obtained by subtracting the curve under diazoxide by the curve under tolbutamide. The arrow indicates the reversal potential of K_{ATP} currents. Histograms summarizing the K_{ATP} current reversal potential (**E, F**) and relative K_{ATP} conductance (**G,H**) in identified neuronal subtypes (**E, G**) or between glutamatergic and GABAergic neurons (**F, G**). Data are expressed as mean ± standard error of the mean (SEM), and the individual data points are depicted. n.s., not statistically significant. *, ** and *** indicate statistically significant with $p< 0.05$, 0.01 and 0.001 respectively.

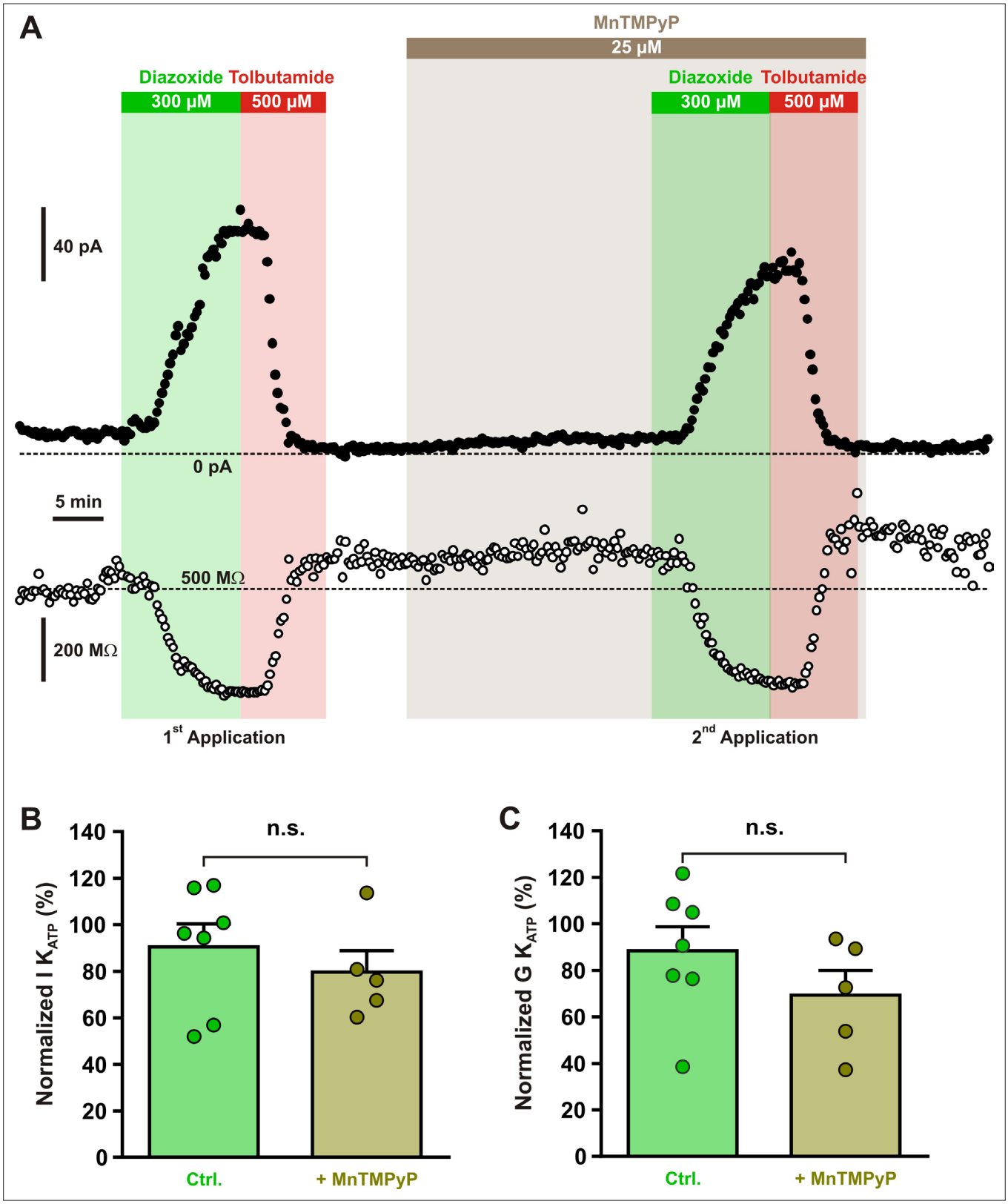

Figure 2—figure supplement 1. Diazoxide-induced current is independent of reactive oxygen species (ROS) production. (**A**) Representative stationary currents at −60 mV (filled circles) and membrane resistance (open circles) changes induced by diazoxide and tolbutamide under control condition and in presence of the superoxide dismutase and catalase mimetic, MnTMPyP. The colored bars and shaded zones indicate the duration of application. Histograms summarizing the relative K_{ATP} currents (**B**) and relative whole-cell K_{ATP} conductance (**C**) evoked by two consecutive diazoxide and tolbutamide

Figure 2—figure supplement 1 continued on next page

Figure 2—figure supplement 1 continued

applications in control condition (Ctrl.) and after the presence of MnTMPyP. Data are normalized by the data measured during first application, expressed as mean ± standard error of the mean (SEM), and the individual data points are depicted. n.s., not statistically significant.

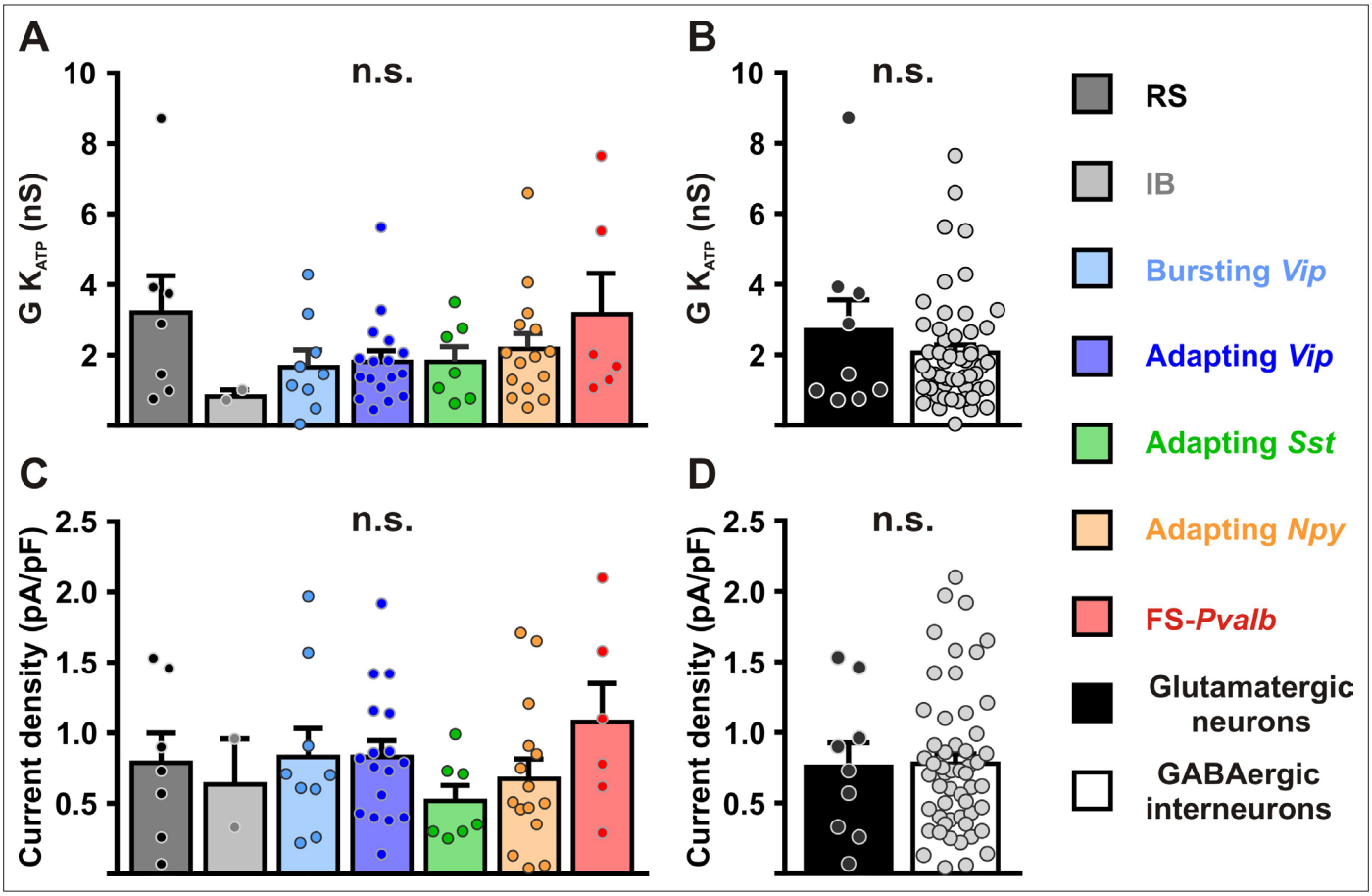

Figure 2—figure supplement 2. Characterization of K_{ATP} channels in different cortical neurons. Histograms summarizing the whole-cell K_{ATP} conductance (**A, B**) and K_{ATP} current density (**C, D**) and K_{ATP} current reversal potential in identified neuronal subtypes (**A,C**) or between glutamatergic and GABAergic neurons (**B,D**). Data are expressed as mean ± standard error of the mean (SEM), and the individual data points are depicted. n.s., not statistically significant.

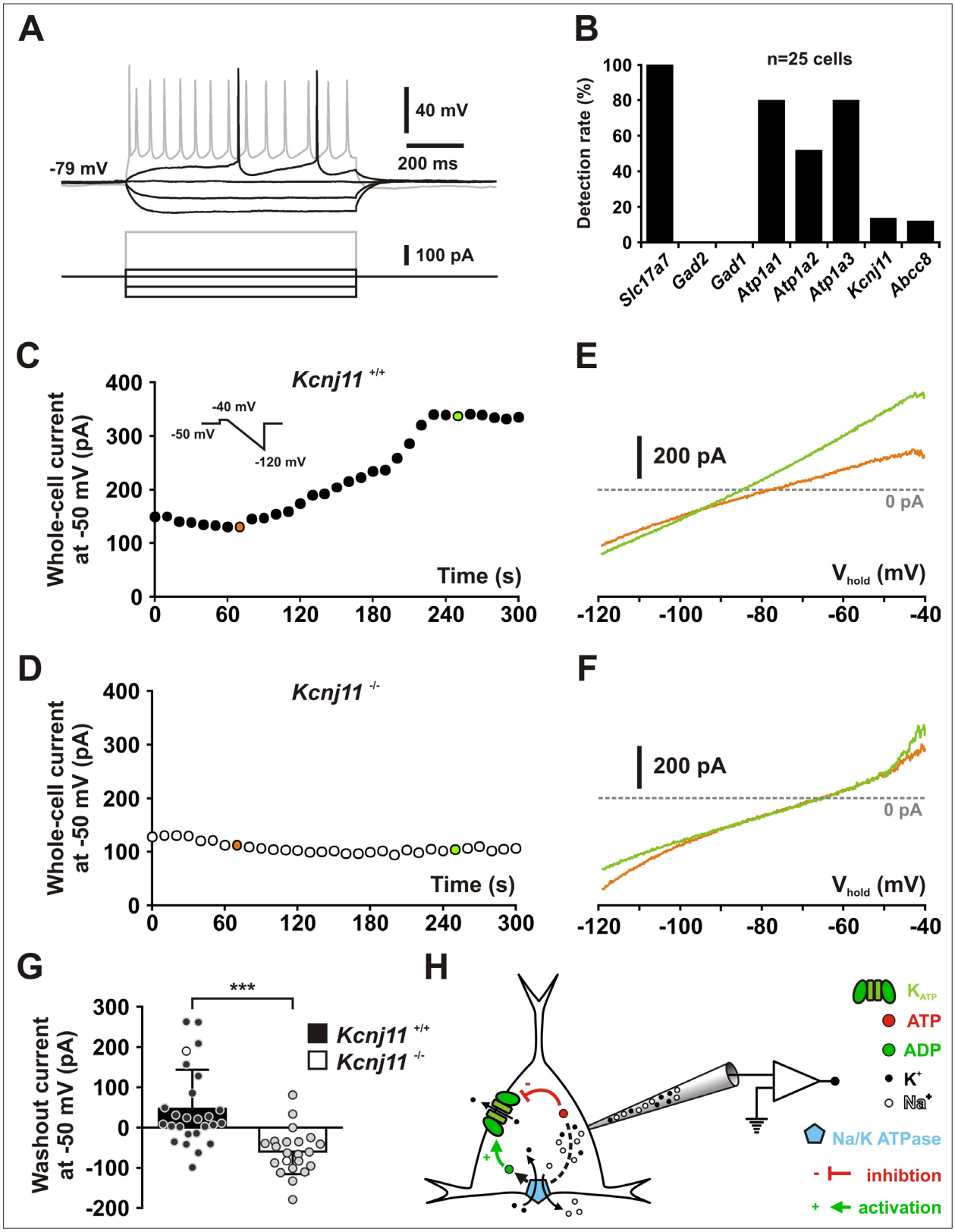

Figure 3. KCNJ11 is the pore-forming subunit of K_{ATP} channels in cortical neurons. (**A**) Representative voltage responses of a mouse layer II/III regular spiking (RS) pyramidal cell induced by injection of current pulses (bottom traces). (**B**) Histograms summarizing the detection rate of *Slc17a7*, *Gad2* and *1*, the *Atp1a1-3* subunits of the Na/K ATPase and the *Kcnj11* and *Abcc8* K_{ATP} channel subunits in layer II/III regular spiking (RS) pyramidal cells from *Kcnj11*$^{+/+}$ mice. (**C, D**) Whole-cell stationary currents recorded at 50 mV during dialysis with ATP-free pipette solution in cortical neurons of *Kcnj11*$^{+/+}$ (**C**)

Figure 3 continued on next page

Figure 3 continued

and *Kcnj11*$^{-/-}$ (**D**) mice. Inset: voltage clamp protocol. (**E, F**) Current–voltage relationships obtained during ATP washout at the time indicated by green and orange circles in (**C, D**) in cortical neurons of *Kcnj11*$^{+/+}$ (**E**) and *Kcnj11*$^{-/-}$ (**F**) mice. (**G**) Histograms summarizing the whole-cell ATP washout currents in *Kcnj11*$^{+/+}$ (black) and *Kcnj11*$^{-/-}$ (white) cortical neurons. Data are expressed as mean ± standard error of the mean (SEM), and the individual data points are depicted. Open symbols in *Kcnj11*$^{+/+}$ and *Kcnj11*$^{-/-}$ bar plots indicate the cells illustrated in (**C, D**) and (**E, F**), respectively. (**H**) Diagram depicting the principle of the ATP washout experiment. *** indicates statistically significant with $p < 0.001$.

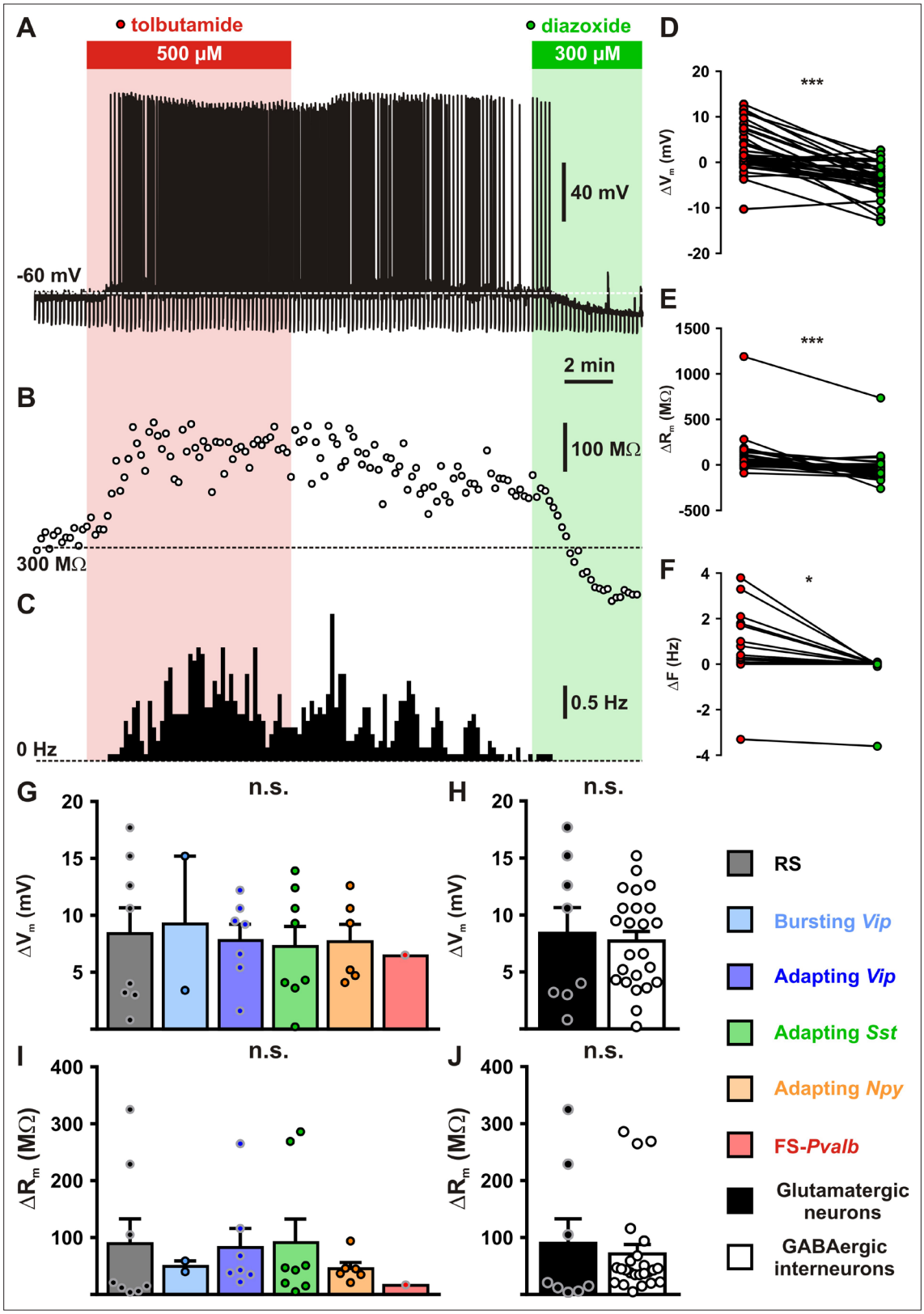

Figure 4. Modulation of cortical neuronal excitability and activity by K_{ATP} channels. Representative example of a regular spiking (RS) neurons showing the changes in membrane potential (**A**), resistance (B, open circles) and spiking activity (**C**) induced by application of tolbutamide (red) and diazoxide (green). The colored bars and shaded zones indicate the application duration of K_{ATP} channel modulators. Relative changes in membrane potential (**D**), resistance (**E**), and firing rate (**F**) induced by tolbutamide and diazoxide in cortical neurons. Histograms summarizing the modulation of membrane

Figure 4 continued on next page

Figure 4 continued

potential (G, $H_{(5,32)}$ = 0.15856, p = 0.999, and H, $U_{(8,24)}$ = 96, p = 1.0000) and resistance (I, $H_{(5,32)}$ = 2.7566, p = 0.737, and J, $U_{(8,24)}$ = 73, p = 0.3345) by K_{ATP} channels in neuronal subtypes (**G, I**) and groups (**H, J**). Data are expressed as mean ± standard error of the mean (SEM), and the individual data points are depicted. n.s., not statistically significant. * and *** indicate statistically ignificant with p<0.05 and 0.001.

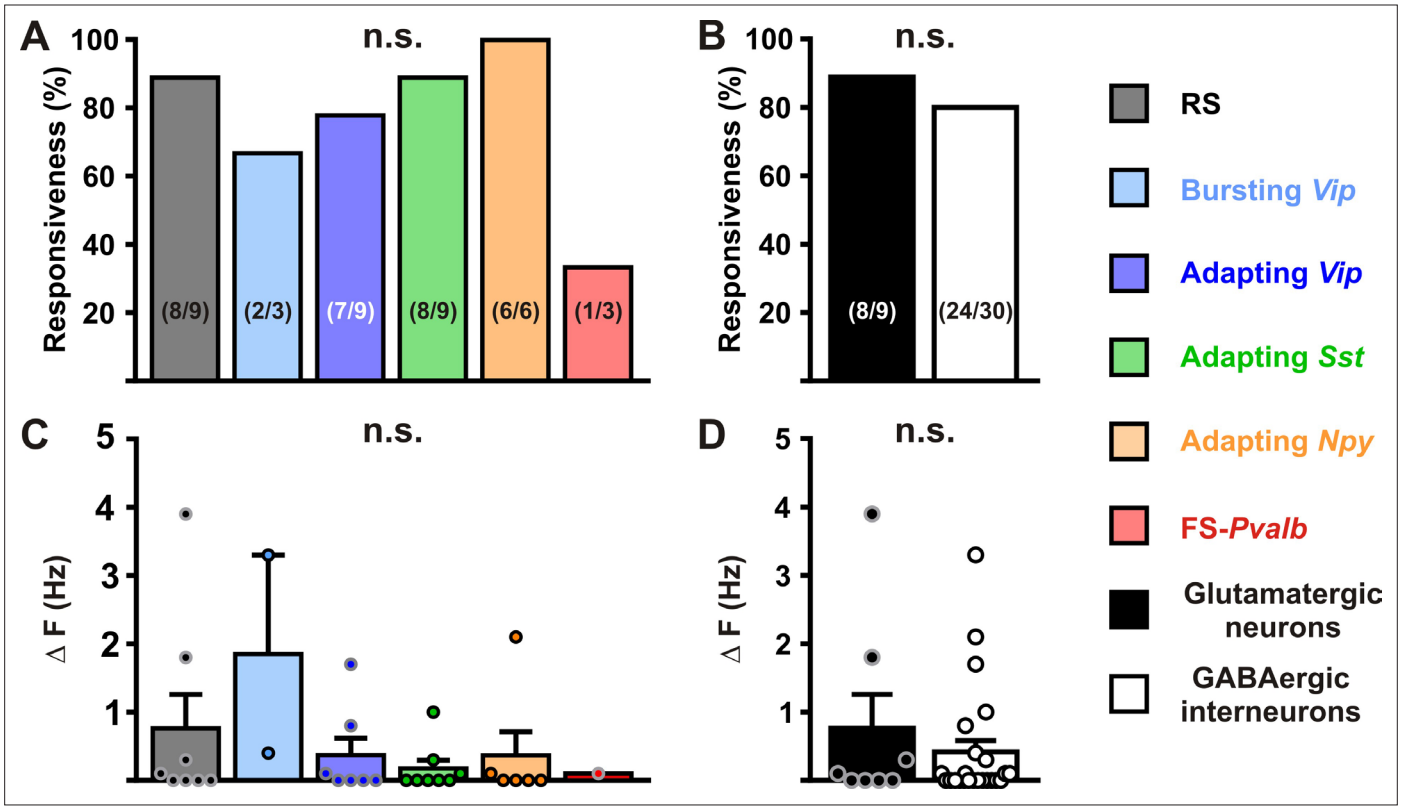

Figure 4—figure supplement 1. Modulation of neuronal activity in different cortical neurons by K_{ATP} channels. Histograms summarizing the proportion of responsive neurons (A, $K^2_{(5)}$ = 7.3125, p = 0.1984, and B, p = 1.0000) and modulation firing rate (C, $H_{(5,32)}$ = 5.0202, p = 0.413, and D, $U_{(8,24)}$ = 87, p = 0.7169) by K_{ATP} channels in neuronal subtypes (**A, C**) and groups (**B, D**). The numbers in brackets indicate the number of responsive cells and analyzed cells, respectively. Data are expressed as mean ± standard error of the mean (SEM), and the individual data points are depicted. n.s., not statistically significant.

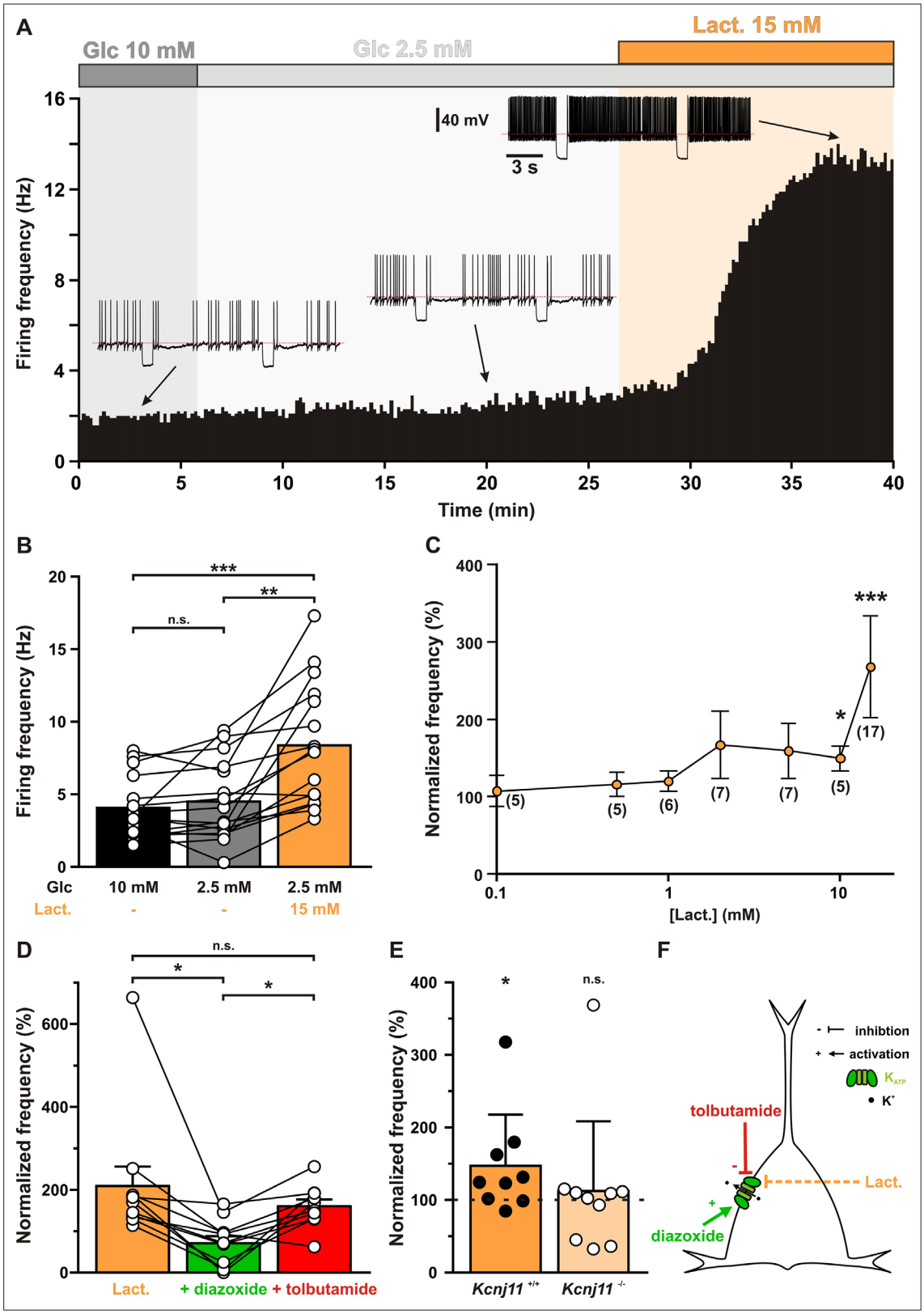

Figure 5. Lactate enhances cortical neuronal activity via K_{ATP} channel modulation. (**A**) Representative perforated patch recording of an adapting vasoactive intestinal polypeptide (VIP) neuron showing the modulation of firing frequency induced by changes in the extracellular concentrations of metabolites. The colored bars and shaded zones indicate the concentration in glucose (gray) and lactate (orange). Voltage responses recorded at the time indicated by arrows. The red dashed lines indicate −40 mV. (**B**) Histograms summarizing the mean firing frequency during changes in extracellular

Figure 5 continued on next page

Figure 5 continued

concentration of glucose (black and gray) and lactate (orange). Data are expressed as mean ± standard error of the mean (SEM), and the individual data points are depicted. n.s., not statistically significant. *, ** and *** indicate statistically significant with $p< 0.05$, 0.01 and 0.001, respectively. (**C**) Dose-dependent enhancement of firing frequency by lactate. Data are normalized by the mean firing frequency in absence of lactate and are expressed as mean ± SEM. Numbers in brackets indicate the number of recorded neurons at different lactate concentrations. (**D**) Histograms summarizing the normalized frequency under 15 mM lactate (orange) and its modulation by addition of diazoxide (green) or tolbutamide (red). Data are expressed as mean ± SEM, and the individual data points are depicted. n.s., not statistically significant. (**E**) Histograms summarizing the enhancement of normalized frequency by 15 mM lactate in *Kcnj11*$^{+/+}$ (orange) and *Kcnj11*$^{-/-}$ (pale orange) mouse cortical neurons. The dash line indicates the normalized mean firing frequency in absence of lactate. Data are expressed as mean ± SEM, and the individual data points are depicted. (**F**) Diagram depicting the enhancement of neuronal activity by lactate via modulation of K_{ATP} channels.

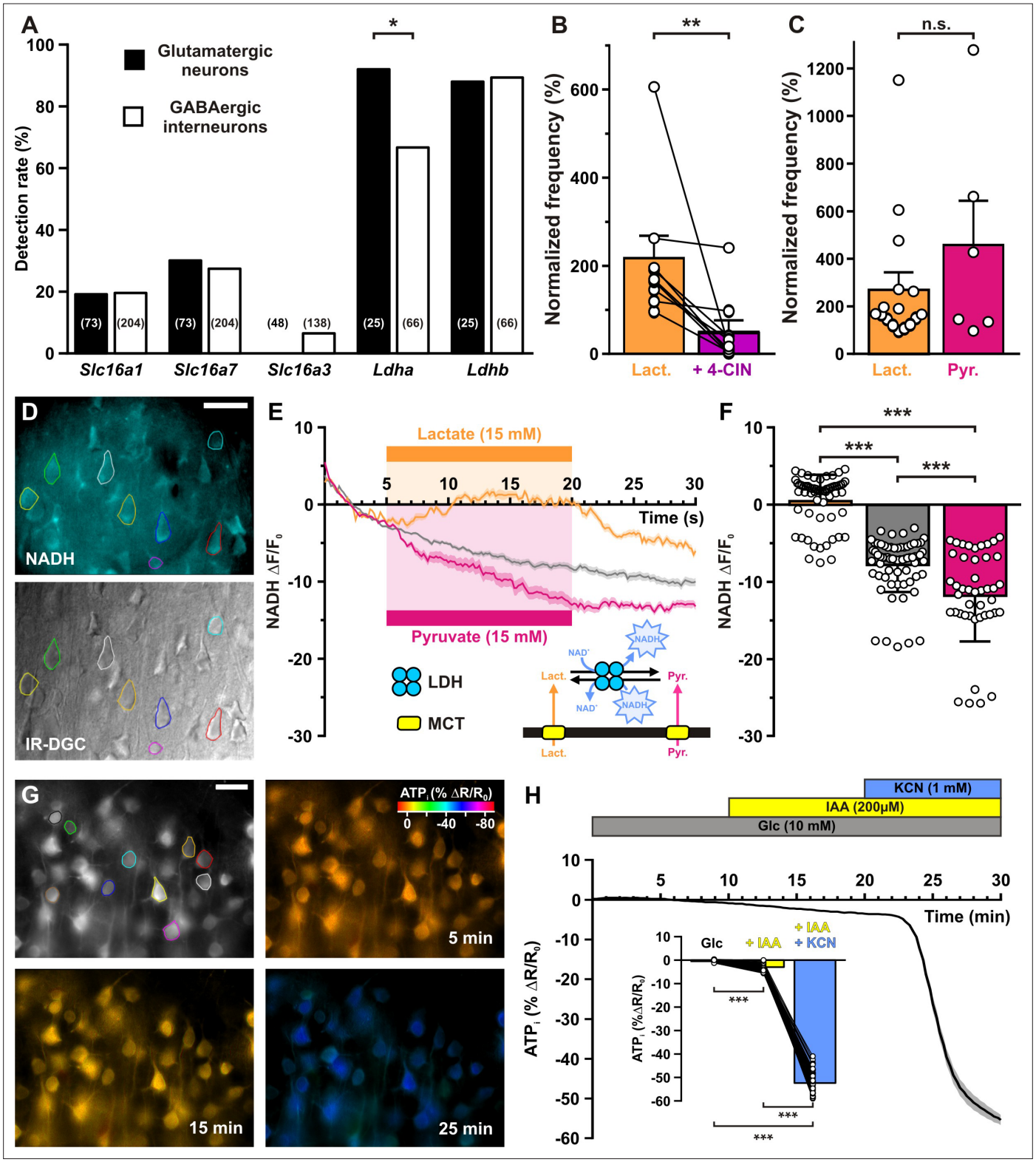

Figure 6. Lactate enhancement of cortical neuronal activity involves lactate uptake and metabolism. (**A**) Histograms summarizing the detection rate of the monocarboxylate transporters *Slc16a1*, *7*, and 3 and *Ldha* and *b* lactate dehydrogenase subunits in glutamatergic neurons (black) and GABAergic interneurons (white). The numbers in brackets indicate the number of analyzed cells. (**B**) Histograms summarizing the enhancement of normalized frequency by 15 mM lactate (orange) and its suppression by the monocarboxylate transporters (MCTs) inhibitor α-cyano-4-hydroxycinnamic acid (4-CIN; purple). Data are expressed as mean ± standard error of the mean (SEM), and the individual data points are depicted. (**C**) Histograms summarizing

Figure 6 continued on next page

Figure 6 continued

the enhancement of normalized frequency by 15 mM lactate (orange) and pyruvate (magenta). Data are expressed as mean ± SEM, and the individual data points are depicted n.s., not statistically significant. (**D**) Widefield NADH (reduced form of nicotinamide adenine dinucleotide) autofluorescence (upper panel, scale bar: 20 µm) and corresponding field of view observed under IR-DGC (lower panel). The somatic regions of interest are delineated. (**E**) Mean relative changes in NADH autofluorescence in control condition (gray) and in response to 15 mM lactate (orange) or pyruvate (magenta). The colored bars indicate the duration of applications. Data are expressed as mean ± SEM. Inset: diagram depicting the NADH changes induced by lactate and pyruvate uptake by MCT and their interconversion by lactate dehydrogenase (LDH). (**F**) Histograms summarizing the mean relative changes in NADH autofluorescence measured during the last 5 min of 15 mM lactate (orange) or pyruvate (magenta) application and corresponding time in control condition (gray). Data are expressed as mean ± SEM, and the individual data points are depicted. (**G**) Widefield YFP fluorescence of the ATP biosensor AT1.03^{YEMK} (upper left panel, scale bar: 30 µm) and pseudocolor images showing the intracellular ATP (YFP/CFP ratio value coded by pixel hue, see scale bar in upper right panel) and the fluorescence intensity (coded by pixel intensity) at different times under 10 mM extracellular glucose (upper right panel) and after addition of iodoacetic acid (IAA; lower left panel) and potassium cyanide (KCN; lower right panel). (**H**) Mean relative changes in intracellular ATP (relative YFP/CFP ratio) measured under 10 mM extracellular glucose (gray) and after addition of IAA (yellow) and KCN (blue). Data are expressed as mean ± SEM. The colored bars indicate the time and duration of metabolic inhibitor application. Inset: Histograms summarizing the mean relative changes in intracellular ATP (relative YFP/CFP ratio) ratio under 10 mM extracellular glucose (gray) and after addition of IAA (yellow) and KCN (blue). Data are expressed as mean ± SEM, and the individual data points are depicted. *, ** and *** indicate statistically significant with $p< 0.05$, 0.05 and 0.001, respectively.

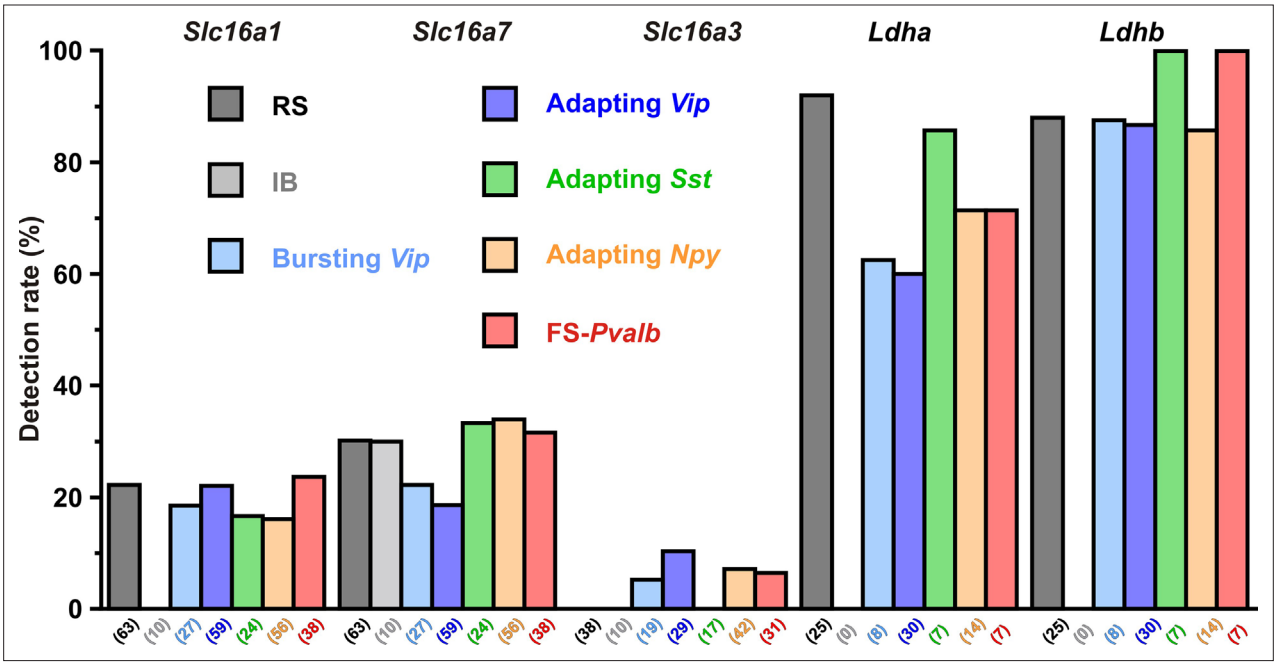

Figure 6—figure supplement 1. Detection rate of monocarboxylate transporters and lactate dehydrogenase subunits in different cortical neuronal types. Histograms summarizing the detection rate of the monocarboxylate transporterMCTs Slc16a1, 7, and 3 and Ldha and b LDHlactate dehydrogenase subunits in different neuronal subtypes. The numbers in brackets indicate the number of analyzed cells.

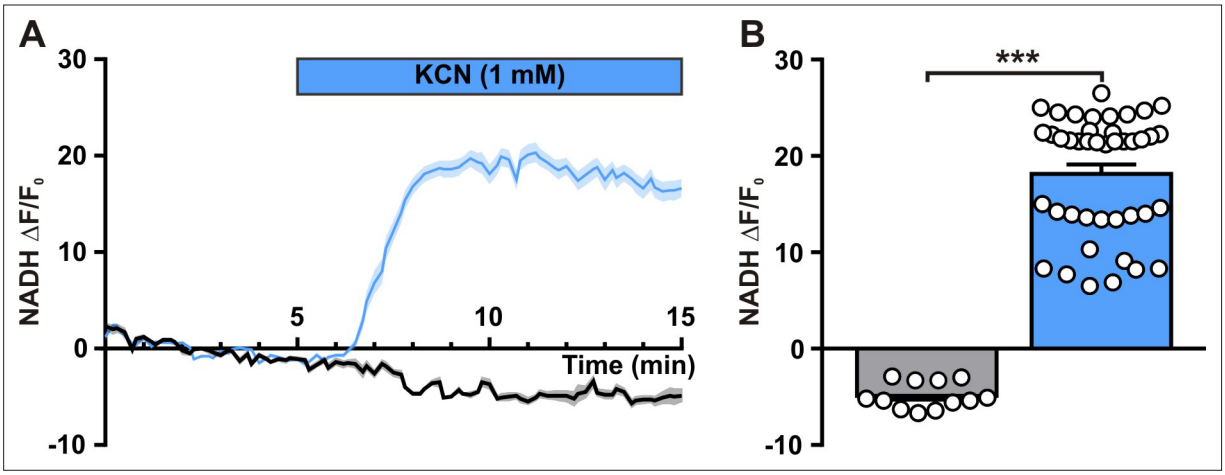

Figure 6—figure supplement 2. Neuronal NADH autofluorescence increase by blockade of oxidative phosphorylation. (**A**) Mean relative changes in NADH autofluorescence in control condition (gray) and in response to 1 mM potassium cyanide (KCN; blue). The colored bar indicates the duration of KCN applications. Data are expressed as mean ± SEM. (**B**) Histograms summarizing the mean relative changes in NADH autofluorescence measured during the last 5 min of 1 mM KCN application (blue) and corresponding time in control condition (gray). Data are expressed as mean ± SEM, and the individual data points are depicted. *** indicates statistically significant with $p < 0.001$.

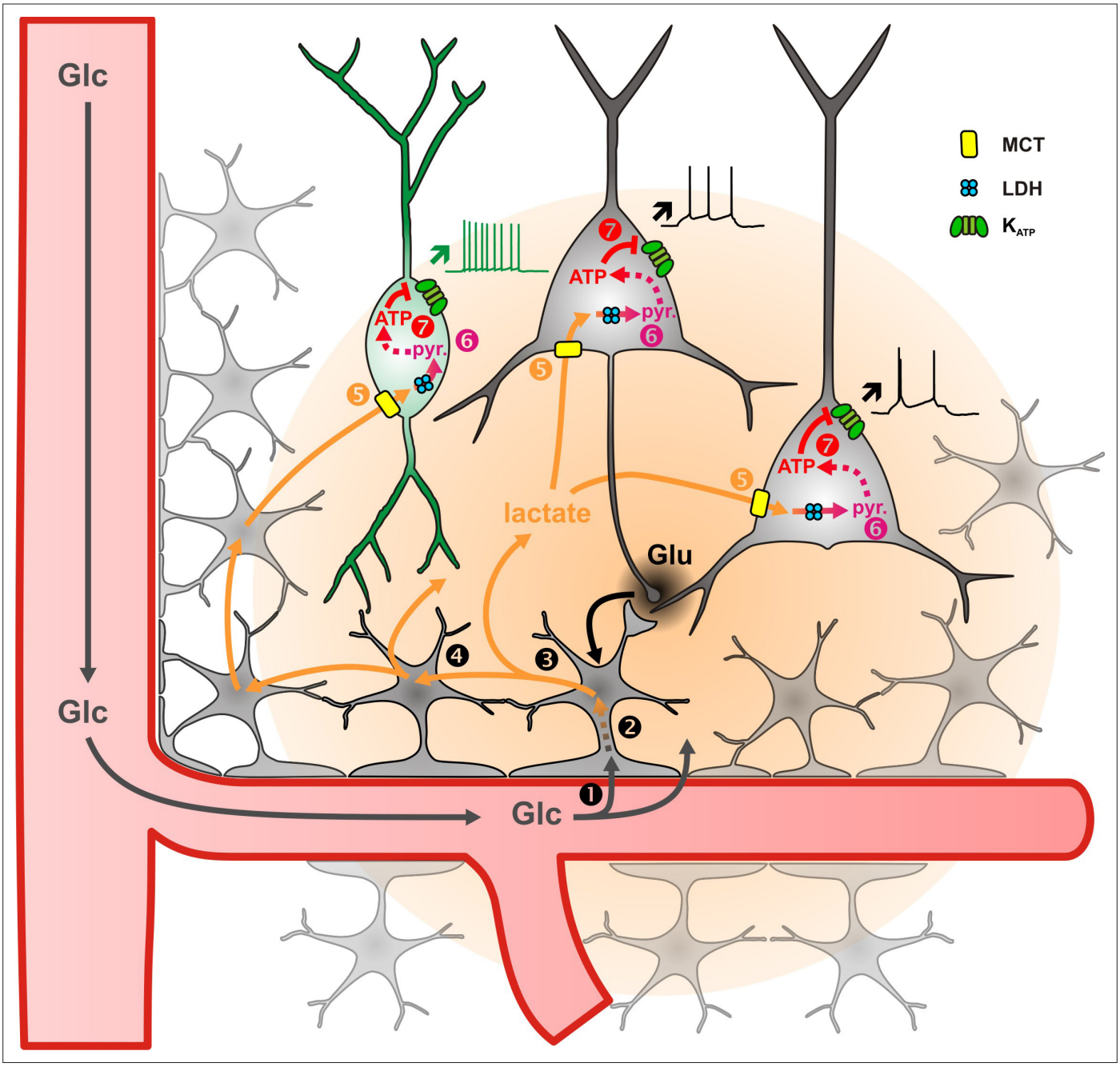

Figure 7. Diagram summarizing the mechanism of lactate sensing in the cortical network. Glutamate (Glu) released during synaptic transmission stimulates (1) blood glucose (Glc) uptake in astrocytes, (2) aerobic glycolysis, (3) lactate release, and (4) diffusion through the astrocytic network. Lactate is then (5) taken up by neurons via monobarboxylate transporters (MCT) and (6) oxidized into pyruvate by lactate dehydrogenase (LDH). The ATP produced by pyruvate oxidative metabolism (7) closes KATP channels and increases the spiking activity of both pyramidal cells (black) and inhibitory interneurons (green). The color gradient of the circles represents the extent of glutamate (black) and lactate (orange) diffusion, respectively. Dashed arrows indicate multisteps reactions.